ACS Partner Journal

CHEMICAL & BIOMEDICAL IMAGING

Open Access

This article is licensed under CC-BY-NC-ND 4.0

pubs.acs.org/ChemBioImaging

Review

The Bioimaging Story of AIEgens

Siyuan Wang,[#] Kun Zhou,[#] Xinyan Lyu, Haowen Li, Zijie Qiu,[*] Zheng Zhao,[*] and Ben Zhong Tang[*]

Cite This: *Chem. Biomed. Imaging* 2023, 1, 509–521

Read Online

ACCESS | Metrics & More | Article Recommendations

ABSTRACT: Observations of the micro world, especially the structures of organelles, have been attractive topics since the 17th century. As a powerful detection tool, the fluorescence technique has played a significant role in bioimaging to provide more details and enhance the signal-to-noise ratio compared to that of traditional optical microscopes. The boom of aggregate-induced emission luminogens (AIEgens) in the last two decades has revolutionized the design strategy of luminescent materials for biological applications. This Review summarizes the advantages and recent progress of AIEgens in imaging and tracking. Different imaging strategies of AIEgens including turn-on imaging, stimuli-response sensing, and long-term tracking are presented. NIR AIEgens used for in-depth bioimaging via different methods are also discussed. Finally, we propose several potential development directions for AIEgens in bioimaging.

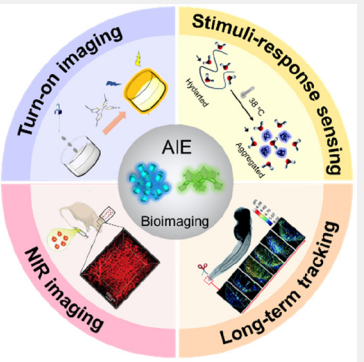

KEYWORDS: *aggregate-induced emission, bioimaging, fluorescence imaging, visualization, turn-on imaging, stimuli-response sensing, long-term tracking, NIR imaging*

1. INTRODUCTION

For a long time, curiosity has driven people to observe tiny things invisible to the naked eye. As early as the first century A.D., Seneca, the tutor of the emperor Nero, once discovered the phenomenon of enlarging letters underwater. In the 17th century, the first telescope was invented by Italian scientist Galileo Galilei, which can see "flies as large as hens."[1,2] However, human curiosity did not stop there. Compared to static objects, the observation of living creatures was much more attractive. Anton von Leeuwenhoek improved the microscope and used it to observe various tiny creatures.[3] Until then, the door of the microbial world had gradually opened to humans. The microscope allowed people to observe various cellular organelles, such as mitochondria, chloroplasts, etc.[4−6] On the other hand, most of the components in the cell structure are colorless and transparent, making it difficult for human eyes to distinguish them under ordinary optical microscopes. One strategy to improve the imaging contrast and quality is to stain cellular organelles with different dyes that emit fluorescence.

"Fluorescence" was first proposed by George Gabriel Stokes in the 19th century, who also predicted that fluorescence could be used as an analytical tool.[7] The first fluorescence microscopes were invented by the companies Carl Zeiss and Carl Reichert at the beginning of the 20th century.[8] With its distinctive advantages of noninvasiveness, high sensitivity, and real-time response, fluorescence imaging has become an irreplaceable detection method in biological and medical research.[9,10] In recent years, plenty of fluorescent materials have been developed for bioimaging, like metal nanoclusters,[11,12] quantum dots,[13,14] and carbon dots.[15,16] Besides these materials, small organic molecules also attracted significant attention due to their excellent biocompatibility, tunable emission wavelengths, and variable functionalization strategies. Since biological systems are an aqueous environment, where organic molecules tend to aggregate, most of the traditional organic fluorophores show weak or even quenched emissions in high-concentration solutions due to $\pi-\pi$ stacking interactions. This phenomenon is known as aggregation-caused quenching (ACQ), which significantly limits the application of ACQ fluorophores in biological systems.[17]

As the opposite of the ACQ effect, Tang and co-workers conceptually coined the aggregation-induced emission (AIE) phenomenon in 2001.[18] Unlike traditional organic dyes, AIEgens have no or weak emissions when dispersed in solution but display strong emissions in the aggregated or solid state. The mechanism of AIE is well explained by the restriction of intramolecular motion (RIM), including restriction of intramolecular rotation (RIR) and restriction of intramolecular vibration (RIV) (Figure 1). When the molecular motion is restricted, the nonradiative decay channel

Received: April 29, 2023
Revised: June 15, 2023
Accepted: June 19, 2023
Published: July 3, 2023

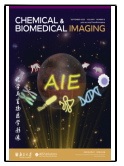

© 2023 The Authors. Co-published by Nanjing University and American Chemical Society

https://doi.org/10.1021/cbmi.3c00056
Chem. Biomed. Imaging 2023, 1, 509−521

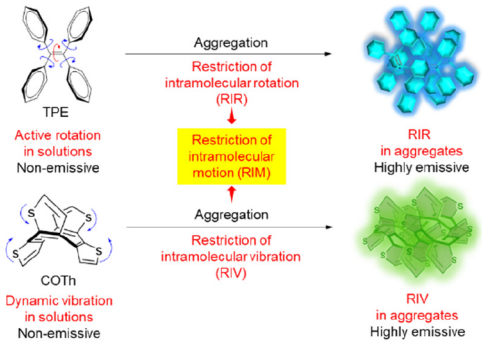

Figure 1. Proposed mechanism of aggregation-induced emission. Reproduced with permission from ref 19. Copyright 2020 Wiley-VCH.

will be blocked, while enhancing the radiative decay channel.[19] The key feature of AIE luminogens, that is, embracing the aggregation effect rather than avoiding it, makes them intrinsically compatible with applications in biological systems, where AIEgens are in the aggregated state. In this way, the emission from aggregate is much brighter than single molecule or dilute solution, which endows AIEgens the first advantage compared to traditional dyes. In addition, aggregate units many molecule together makes AIEgens excellent antibleaching abilities, which is indispensable property for monitoring long time biobehavior.[20] Applicability to living organisms, bright emission, and antibleaching ability provide AIEgens promising development prospects. The explosive development of AIE research has revolutionized the design strategy of luminescent materials for biomedical applications in organelle imaging, biological process tracing, as well as multimode synergetic therapy in the past two decades.[21−23]

To comprehensively demonstrate the advantages of AIEgens in the field of bioimaging, in this Review, we summarize several strategies for AIEgen-based bioimaging with some typical examples from the visible light to the near-infrared (NIR) region (Scheme 1). First of all, turn-on imaging will be

Scheme 1. Different Strategies of AIE Probes

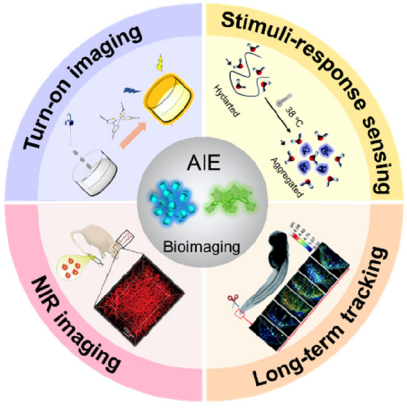

discussed as the most fundamental and essential characteristic of AIE. Stimuli-response sensing will be reviewed as the application for the detection of the physiological environment. In addition, long-term tracking will be explored to observe different biological processes. Furthermore, NIR imaging will be investigated as a representative of deep and precise imaging of living systems. In the end, several promising possibilities for future development in bioimaging will be proposed, including the development of novel imaging techniques and applications. We hope that this Review will provide valuable information and viewpoints for researchers in this field and inspire further exploration of the diverse applications and opportunities offered by AIEgens in this exciting and rapidly evolving field of bioimaging.

2. TURN-ON IMAGING

According to the mechanism of AIE, AIEgens exhibit fluorescence upon restriction of molecular motion, which has led to the development of numerous turn-on AIE probes.[24,25] By utilizing the RIM mechanism, these turn-on probes can selectively detect and visualize various molecular targets with high sensitivity and low background noise, offering a powerful tool for biological research. Traditional ACQ fluorescence probes could have emission even in nontargeted binding sites and culture medium, which result in high background noise. On the contrary, AIEgens have almost no emission in solution. After addition to culture medium, only binding sites can exhibit significant emission, due to AIEgens only generating bright emission colors in the aggregate state, and the background signal in the culture medium is weak, making the bioimaging process wash-free and user-friendly.[26] With the advantages of specific emission at binding sites, low background noise, and convenient wash-free operation, AIEgens are excellent candidates for turn-on imaging probes.

The detection of bacteria by fluorescent dyes was usually through the strategy of the electrostatic adsorption interaction. For example, Phillips, Wang, and Tang et al. reported the cyclooctatetrathiophene (COTh) derivatives, which exhibited restricted vibration upon aggregation and contained unique AIE properties.[27] Experimental and theoretical data demonstrated that intramolecular motion triggered by aromaticity reversal played a pivotal role in the aggregation-induced emission phenomenon of the COTh system. To explore the potential of these molecules for biological imaging applications, a COTh derivative with pyridine substitutions with positive charges (COTh-Py) was designed and synthesized. COTh-Py showed weak emission in an aqueous solution but exhibited a bright emission upon aggregation. When added to the culture medium of bacteria, the positive charges on the COTh-Py molecule electrostatically adsorbed onto the negative charges on the surface of the bacteria, resulting in the restriction of the vibration of the molecule's four arms and a corresponding turn-on of its emission (Figure 2a,b).

Besides electrostatic adsorption, the change from the dispersed state to the aggregated state could be realized via differences in solubility. AIEgens tend to exhibit increased emission upon aggregation in undesirable solvents. By utilizing this strategy, Zhao and Tang et al. developed TPABSM through the construction of triphenylamine (TPA) and benzothiadiazol-7-ylidene malononitrile (BSM) (Figure 2c).[28] TPA was a representative AIEgen endowed with remarkable electron-donating capabilities, while BSM, a newly introduced acceptor core, exhibited a strong electron-accepting ability. By combining TPA and BSM, a donor−acceptor (D-A) structure was formed to empower red emission with excellent AIE properties. Furthermore, the addition of fluorine atoms is a widely used strategy for improving the lipophilicity of organic molecules.[29] Encouraged by this, the authors explored the potential of TPABSM as a lipid droplet (LD) targeting dyes. First, the log P (n-octanol/water partition coefficient) value,

https://doi.org/10.1021/cbmi.3c00056
Chem. Biomed. Imaging 2023, 1, 509−521

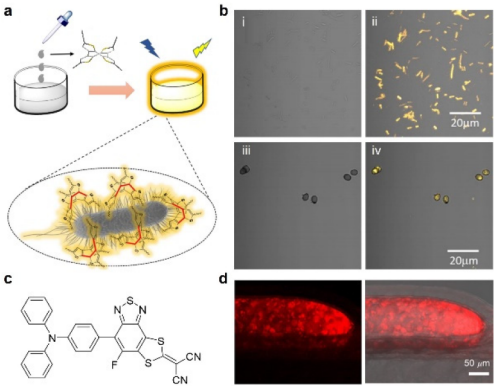

Figure 2. (a) Schematic illustration of the process of bacteria imaging. (b) Microbial imaging application of COTh-Py. (i,ii) Bright-field and fluorescent images of *Escherichia coli* (*E. coli*) with 50 μM of COTh-Py for 1 h. (iii,iv) Bright-field and fluorescent images of *Penicillium chrysogenum* with 20 μM of COTh-Py for 2 h; scale bar is 20 μm. Reproduced with permission from ref 27. Copyright 2019 Springer Nature. (c) Molecule structure of TPABSM. (d) In vivo zebrafish embryo fluorescence and bright merged imaging stained with TPABSM; scale bar is 50 μm. Reproduced with permission from ref 28. Copyright 2022 American Chemical Society.

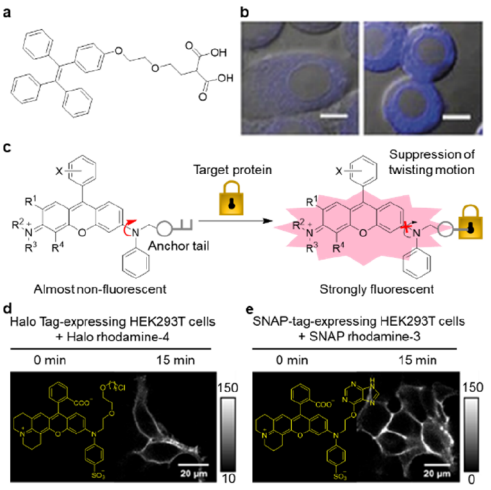

Figure 3. (a) Molecule structure of TPEMA. (b) Confocal images of CK in macrophages without (left) or with (right) pretreated with CK-BB for 30 min and then incubated with TPEMA for 30 min; scale bar is 5 μm. Reproduced with permission from ref 31. Copyright 2020 Wiley-VCH. (c) Design strategies for fluorogenic probes for tag proteins. (d) Time-lapse imaging of HEK293T cells expressing HaloTag-rhodopsin on the cell surface using Halo rhodamine-4 (0.5 μM); scale bar is 20 μm. (e) Time-lapse imaging of HEK293T cells expressing SNAP-tag-ADRβ2 (beta-2 adrenergic receptor) on the cell surface using SNAP rhodamine-3 (0.5 μM); scale bar is 20 μm. Reproduced with permission from ref 32. Copyright 2022 American Chemical Society.

which is related to lipophilicity, of TPABSM was calculated and compared with commercial lipid dyes. The log *P* value of TPABSM was 8.403, higher than those of Nile Red (4.618) and BODIPY 493/503 (5.028), indicating the possibility of TPABSM for LD imaging. Further colocalization experiments verified the specificity of TPABSM for LDs. Consistent with the expected results, TPABSM could stain LDs well in both A549 and HeLa cells. TPABSM was first dissolved in dimethyl sulfoxide (DMSO) with weak emission. After incubating with cells for 1 h, the TPABSM molecules entered and were enriched in LDs because of their brilliant lipophilicity. Finally, the aggregation restricted the rotation of the TPA unit and turned on the emission of TPABSM in cells' LDs. In vivo imaging was also conducted in zebrafish. It is known that the yolk sac of zebrafish is responsible for storing neutral lipids and polar phospholipids.[30] As shown in Figure 2d, after being stained with TPABSM for 30 min, 3-day-old zebrafish embryos displayed vibrant red fluorescence signals that emanated from their yolk sac. This turn-on probe offers a platform for in vivo LD imaging and research on LD-related physiological activities.

Restricting the motion of a molecule by inserting it into a protein cavity is another promising strategy for developing turn-on probes. Zhang, Niu, and Zhang et al. developed a novel AIEgen, TPEMA, by conjugating ethylmalonic acid, a targeting group, with tetraphenylethylene (TPE) (Figure 3a).[31] This innovative AIEgen exhibited high selectivity for specific cytosolic creatine kinase (CK) isomers due to the different cavities of different CK subunits, the B subunit, and the M subunit. Three different CK isomers could be constructed by the homo/heterodimerization of CK-B and CK-M (CK-BB, CK-MB, CK-MM). The detection of TPEMA of different CK isomers was investigated first. TPEMA showed excellent fluorescence as high as 9.2-fold enhancement after adding CK-BB. The Job plot assay indicated that the binding stoichiometry between TPEMA and CK-BB is 1:1, revealing the restriction of single molecular motion. The addition of other types of CK isomers or common biomolecules did not turn on the TPEMA fluorescence. Molecular dynamics (MD) simulation results confirmed the restriction of TPEMA in the B-subunit by strong C−H···π interactions after ethylmalonic acid anchoring CK-BB, resulting in turn-on emission. On the contrary, the distance between the phenyl rings of TPEMA and the methyl groups of Leu 201 was too long to form C−H···π interactions in the M subunit, where the vibration of TPEMA was free, leading to no fluorescence. The high selectivity of TPEMA to the B subunit of CK isomers encouraged researchers to explore its potential as a cell imaging probe. Macrophage was selected for biological applications in which CK-BB mainly distributes. After incubation with TPEMA after 30 min, fluorescence in the macrophage was observed with a 2.8-fold increase compared to the control group (Figure 3b). There was almost no cellular fluorescence in macrophages pretreated with CK inhibitor 1-fluoro-2,4-dinitrobenzene (DNFB) or ethylmalonic acid, where CK isomers' cavity was blocked.

The recognition of cavities with different sizes by the same AIEgen inspired the development of a series of derivative probes for recognizing different proteins using the same luminogen by changing the targeting moiety. Hanaoka et al. proposed that the fluorescence of *N*-alkylated derivatives of rhodamine, commonly used fluorescence dark quenchers, could be turned on by restriction of twisted intramolecular charge transfer (TICT), an effect induced by intramolecular motion.[32,33] Density functional theory (DFT) and time-dependent density functional theory (TD-DFT) calculations tentatively confirmed the correctness of their hypothesis. To further verify their theory, a series of molecules were designed by incorporating the tail of N-Ph rhodamine with an anchor structure that was used to target the protein (Figure 3c). HaloTag and SNAP-tag are two common tags used for covalent labeling inside living cells. HaloTag is an enzyme

https://doi.org/10.1021/cbmi.3c00056
Chem. Biomed. Imaging 2023, 1, 509−521

whose active site can be covalently linked to a chloroalkane ligand to form a mechanically strong bond.[34] SNAP-tag is usually covalently labeled by covalently tagging with an O^6-benzylguanine (BG) derivative with a chemical probe. In this process, the BG derivative reacts irreversibly with the SNAP-tag, resulting in the transfer of the functionalized benzyl group in the BG derivative to a cysteine residue at the active site of the SNAP-tag, resulting in the formation of a covalently modified protein.[35] Halo Tag and SNAP-tag fluorogenic probes were developed for targeting specific proteins, respectively. Docking simulation results revealed that fluorogenic probes would be located near the surface of proteins, effectively suppressing the twisting motion of the xanthene-N bond. As a result, the fluorescence of these probes was turned on and showed significant increases upon the addition of specific proteins (Halo Tag protein and SNAP-tag protein). After the addition of denaturing agents like 1% SDS or 8 M urea, the fluorescence intensity showed a huge decrease, indicating the critical role of protein structure for binding with fluorogenic probes. Among all these fluorogenic probes, two NIR fluorogenic probes, Halo rhodamine-4 and SNAP rhodamine-3, were selected for live cell imaging (Figure 3d,e). They were incubated with HEK293T cells expressing the Halo Tag or SNAP-tag on the cell surfaces. The fluorescence imaging showed excellent signal-to-noise ratios (SNR) without washing out extra probes, and the surface of the targeting protein-expressing cells was clearly sketched. The restriction of TICT provides a new strategy for turn-on AIE probes.

3. STIMULI-RESPONSE SENSING

The living organism is complex and variable. The physiological environment in an organism changes all the time, and changes in the environment can affect the activities of organisms.[36,37] It is essential to detect microenvironment changes that happen to organisms such as polarity, viscosity, pH, and temperature. Up to now, various AIEgens have been developed for stimuli-response sensing, which was used to study variation in life activity.[38]

Polarity plays a pivotal role in the metabolism of organisms. Changes in polarity are noted to be associated with inflammation and cancer.[39] However, due to the complexity of the intracellular environment, the detection of polarity is difficult, especially at the cellular level. The emission properties of AIEgens are sensitive to the microenvironment and thus have been widely utilized for sensing the polarity of the intracellular environment.[38] Bacteria, which exist everywhere in nature and are related to many diseases, could be divided into two groups by Gram stain.[40] Unlike Gram-positive bacteria, which are characterized by a thick peptidoglycan layer, Gram-negative bacteria typically exhibit a much thinner peptidoglycan layer. Furthermore, an outer membrane is a distinctive feature of Gram-negative bacteria that sets them apart from their Gram-positive counterparts. The difference in their membranes could be shown by the difference in polarity. Zhu et al. developed a polarity-sensitive probe (TICT-lipid) to identify the minute difference between the outer and cell membranes (Figure 4d).[41] TICT-lipid exhibited prominent solvatochromic properties. The emission color transferred from green to red with the increasing solvent polarity, revealing its sensitivity to polarity. The authors proposed that the positive charge and long alkyl chains of TICT-lipid facilitate its intercalation into the bilayer of bacterial membranes. In the

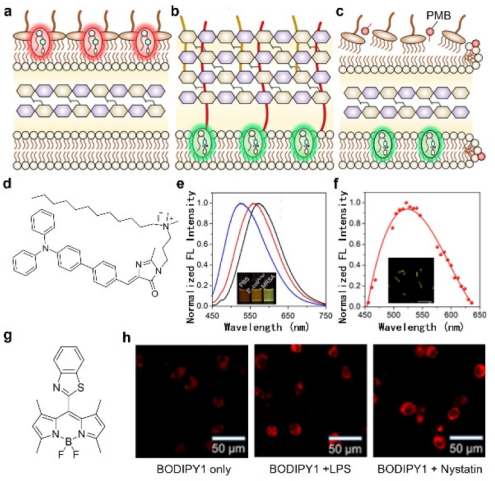

Figure 4. Schematic illustration showing the intercalation of TICT-lipid with (a) Gram-negative and (b) Gram-positive bacteria. (c) Schematic illustration showing the fluorescence responses of TICT-lipid to the disruption effect of PMB on the outer membrane of Gram-negative bacteria. (d) Molecule structure of TICT-Lipid. (e) Normalized emission spectra of TICT-lipid postincubation with PBS (gray), *E. coli*^{Ampr} (red), and MRSA (blue). Inset: Photograph taken under a 365 nm UV lamp (from left to right: PBS, *E. coli*^{Ampr}, MRSA). (f) In situ emission spectra extracted from a panel of the inset. Inset: fluorescence image of *E. coli*^{Ampr} postincubation with PMB at concentrations of 4 μg mL^{-1}; scale bar is 10 μm. Reproduced with permission from ref 41. Copyright 2022 American Chemical Society. (g) Molecule structure of BODIPY1. (h) Fluorescence images of SH-SY5Y cells, which were pretreated with none, LPS, or nystatin (20 μM) for 40 min and then treated with BODIPY1 (5 μM) for another 30 min; scale bar is 50 μm. Reproduced with permission from ref 50. Copyright 2022 American Chemical Society.

loosely packed outer membrane of Gram-negative bacteria, TICT-lipid adopted a highly twisted conformation (Figure 4a). In contrast, TICT-lipid exhibited a less twisted conformation in the membrane of Gram-positive bacteria (Figure 4b). To evaluate the interaction of TICT-lipid with bacterial membranes, the study employed Gram-negative ampicillin-resistant *E. coli*^{Ampr} and Gram-positive methicillin-resistant *Staphylococcus aureus* (MRSA) as representatives of Gram-negative and Gram-positive bacteria, respectively. The emission spectra of TICT-lipid were measured in the presence of these bacteria (Figure 4e). Compared to phosphate-buffered saline (PBS), the incubation of TICT-lipid with bacteria made the emission spectra blue-shifted. The MRSA group exhibited a more pronounced change (ca. 50 nm) compared to the *E. coli*^{Ampr} group (ca. 15 nm). Then, TICT-lipid was used to study the antibacterial mechanism of membrane-disrupting antibiotics. PMB, a cationic peptide, was used as a model drug to disrupt the outer membrane of Gram-negative bacteria. After treatment by PMB, the outer membrane was broken, and TICT-lipid in the outer membrane could enter the cell membrane with a different conformation (Figure 4c). The difference was observed by in situ emission spectra (Figure 4f). With the concentration of PMB increased from 0 to 4 μg mL^{-1}, the fluorescence enhanced and the emission maximum blue-shifted by ca. 20 nm.

Intracellular viscosity is related to many cell progress, like ferroptosis,[42] autophagy,[43] and apoptosis,[44] therefore, the detection of intracellular viscosity is critical. Fluorescence imaging exhibits unparalleled advantages compared to tradi-

https://doi.org/10.1021/cbmi.3c00056
Chem. Biomed. Imaging 2023, 1, 509−521

tional detection methods like chromatography, electroanalysis, etc., which require expensive instruments and complex preparation.[45] Among different design strategies of viscosity-response fluorescence probes, the structure of the molecular rotor is a crucial point that coincides with the philosophy of AIE.[46] Many AIEgens have been developed to sense intracellular viscosity.[47−49] For example, Shi and Yan et al. reported a novel AIEgen for imaging lysosomal viscosity.[50] Several probes based on boron dipyrromethenes (BODIPYs) have been reported for viscosity sensing, depending on the rotation of *meso*-groups.[51,52] Similarly, they designed a new molecule (BODIPY1) with a lysosomal targeting group (Figure 4g). This molecule exhibited an excellent viscosity response and remarkable AIE properties, making it a valuable material for imaging applications. Subcellular imaging has proven its ability to target lysosomes in human neuroblastoma cells (SH-SY5Y cells). After lipopolysaccharide (LPS) or nystatin was added, BODIPY1 was used for sensing the difference in intracellular viscosity. BODIPY1 showed weak emission in low viscous cells but enhanced emission in drug-treated cells (Figure 4h). Through the change of rotators with different targeting abilities, AIEgens can be applied for sensing cellular viscosity in different environments and cells.

pH is an essential parameter in living organisms. Abnormal intracellular pH is connected with cell apoptosis,[53] tissue acidification,[54] and cancer.[55] The color changes of pH-response fluorescence probes in different pH environments are widely used for intracellular pH sensing. AIEgens, with good antiphotobleaching properties, can also be used for sensing intracellular pH.[56] Tang et al. developed dihydroberberine (dhBBR) as a pH-response AIEgen.[57] The great AIE property of dhBBR could be explained by RIV. The nonplanar conformation of dhBBR in the crystal state made molecular vibrations possible. The nitrogen atom is the pH-response site, which is easily protonated in a high-pH environment. The emission color of dhBBR changes from blue at low pH to green at high pH (Figure 5a). This property was used for imaging A549 cells in PBS buffers with different pH. There was no emission in cells incubated in low pH PBS buffer but strong green emission when the pH increased to 7.4 (Figure 5b). Benefiting from its excellent ability for intracellular pH sensing, dhBBR was well employed for visualizing the semipermeability of the cell membrane. In addition, compared to Curcumin, dhBBR exhibited remarkable antiphotobleaching ability after 200 s of irradiation (Figure 5c). AIEgens provide a brighter and more stable platform for intracellular pH sensing.

Besides pH, temperature is another factor associated with biological activities.[58] All biological activities are accompanied by a certain amount of heat exchange. Pathological cells can have higher temperatures due to increased metabolic activity compared to normal cells.[59] It is important to map the intracellular temperature of living cells to detect abnormal areas. Fluorescent thermometers have been developed in the past few years. AIE thermometers attracted great attention attributed to their photostability and biocompatibility.[60,61] Mukhopadhyay, Bauri, and De et al. revealed the photophysical characteristics of well-known thermoresponsive poly(*N*-vinylcaprolactam) (PNVCL).[62] PNVCL showed appealing temperature-dependent phase transition behavior, which is due to the broken hydrogen bonding between the C═O groups and water molecules (Figure 5d). The stable hydrogen bonding formed PNVCL chains into stretched conformations in water. When the temperature increased up to 38 °C, hydrogen bonds

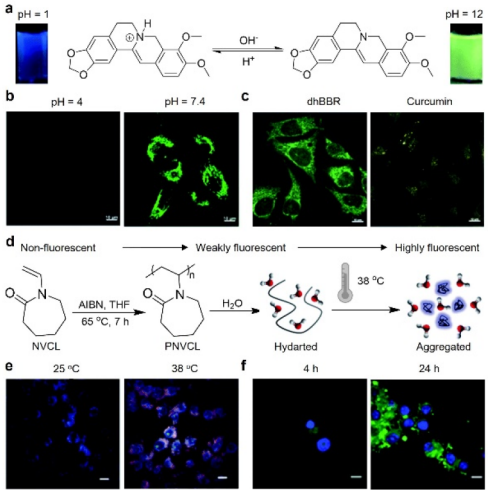

Figure 5. (a) Schematic illustration of dhBBR's fluorescent response to pH change. (b) Fluorescence images of A549 cells stained with dhBBR (1 μM) in PBS buffer with different pH values for 30 min; scale bar is 10 μm. (c) Fluorescence images of HeLa cells stained with dhBBR (1 μM) and curcumin (1 μM) after 200 s of light irradiation; scale bar is 10 μm. Reproduced with permission from ref 57. Copyright 2020 the Royal Society of Chemistry. (d) Synthesis of PNVCL and its thermoinduced conformational transformation. (e) Fluorescence images of MCF-7 cells labeled with PNVCL (250 μg mL^{-1}) at 25 and 38 °C for 24 h; scale bar is 10 μm. (f) Fluorescence images of MCF-7 cells after incubating with 500 μg mL^{-1} PNVCL for different time intervals at 38 °C; scale bar is 10 μm. Reproduced with permission from ref 62. Copyright 2020 the Royal Society of Chemistry.

would be broken, and PNVCL chains would form clusters according to hydrophobic interaction. Different from previous work, the authors focused on the photophysical characteristics of PNVCL. The emission of PNVCL enhanced with an increasing polymer concentration in both THF and water, showing AIE properties. PNVCL also exhibited red-shifting of emission maximum with the increase of excitation wavelength. Without any conventional chromophores, this phenomenon could be explained by the clustering-triggered emission (CTE) mechanism.[63,64] Clusteroluminescence is a prevalent phenomenon observed in nonconventional luminogens that contain heteroatoms with a lone pair of electrons or specific functionalities, such as C═C, C═O, and C≡N.[64] In the case of PNVCL, the nonconventional chromophore moiety, specifically C═O groups with π-electrons or a lone pair of electrons and N atoms with a lone pair of electrons of one cyclic amide, come into close proximity with another amide to form an aggregated cluster. This clustering leads to chromophores that exhibit effective through-space electronic communication, resulting in extended electron delocalization and a rigidified conformation. The rigidity of the molecular conformation restricts vibration and molecular rotation, effectively suppressing nonradiative relaxation. As a result, the polymer exhibits significant emission upon irradiation in the aggregated state. PNVCL was used to sense the intracellular temperature of the MCF-7 cells. When the temperature increased from 25 to 38 °C, the fluorescence was significantly enhanced in all three channels (blue, green, and red) (Figure 5e). In addition, with increasing incubation time ranging from 4 to 24 h, the fluorescence from MCF-7 cells increased under the green channel (Figure 5f). The

https://doi.org/10.1021/cbmi.3c00056
Chem. Biomed. Imaging 2023, 1, 509−521

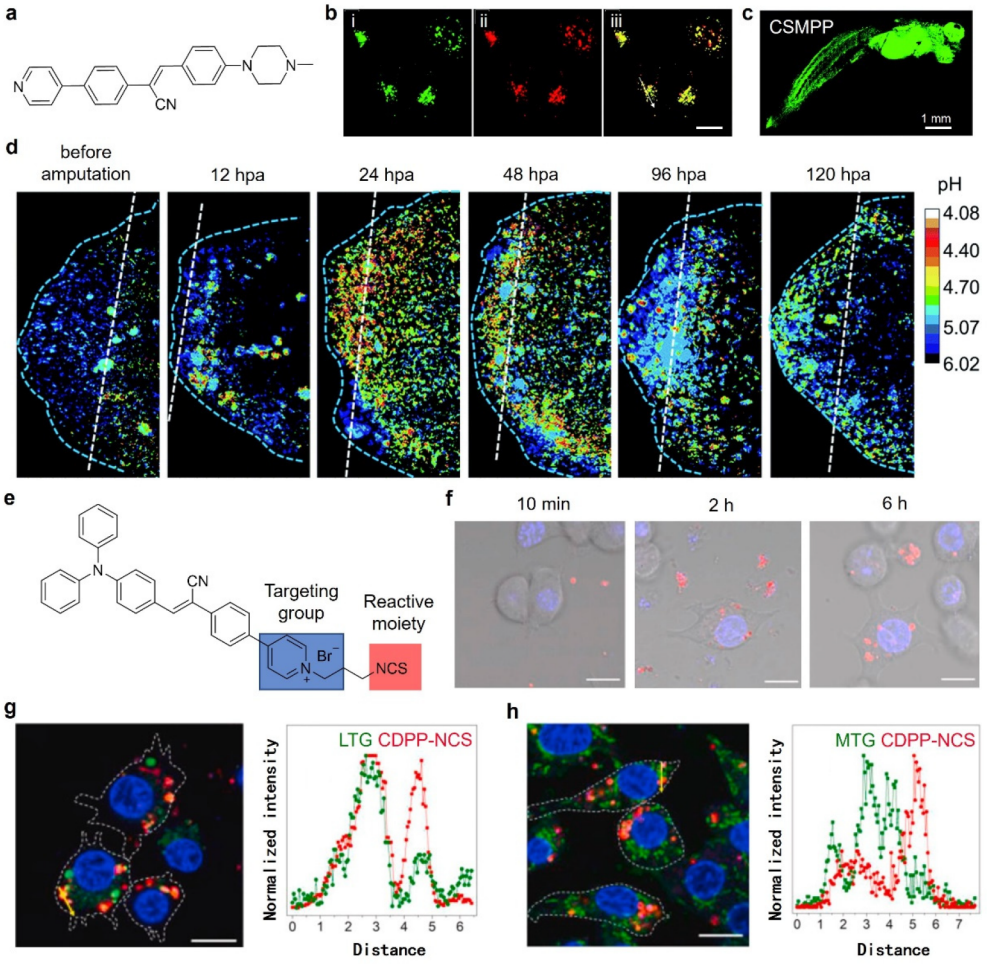

Figure 6. (a) Molecule structure of CSMPP. (b) Fluorescence images of HeLa cells with 200 nM LysoTracker Red (LTR) for 10 min and then costained with 2 μM CSMPP for 10 min. Fluorescence images of (i) CSMPP; (ii) LTR; (iii) merged (a) and (b); scale bar is 10 μm. (c) Fluorescence image of the whole body of the medaka larva after being fed with CSMPP for 4 h; scale bar is 1 mm. (d) Fluorescence images of the medaka larva's caudal fin before amputation and after amputation at different times (12, 24, 48, 96, and 120 hpa); scale bar is 50 μm. Reproduced with permission from ref 70. Copyright 2020 Royal Society of Chemistry. (e) Molecule structure of CDPP-NCS. (f) Fluorescence image of RAW264.7 macrophages incubated with CDPP-NCS labeled *S. aureus* (red) at different times. [CDPP-NCS] = 10 μM; [Hoechst 33342] = 1 μM; scale bar is 10 μm. (g) Fluorescence image of CDPP-NCS labeled *S. aureus* (red) and lysosomes (green) stained with LysoTracker Green (LTG) after incubation for 6 h and the fluorescence intensity profiles in the yellow arrow from the image; scale bar is 10 μm. (h) Fluorescence image of CDPP-NCS labeled *S. aureus* (red) and lysosomes (green) stained with MitoTracker Green (MTG) after incubation for 6 h and the fluorescence intensity profiles in the yellow arrow from the image; scale bar is 10 μm. Reproduced with permission from ref 74. Copyright 2022 Elsevier.

coincubation results with DAPI (a commercial cell nucleus tracker) also indicated PNVCL localized in the cytoplasm without any transfer.

4. LONG-TERM TRACKING

Besides sensing the physiological environment in organisms, long-term tracking of biological activities could reveal more life information and provide a platform for in-depth biological study.[65] Benefit to strong antiphotobleaching ability, intense fluorescence, and great biocompatibility, AIEgens are excellent candidates for *in vivo* long-term tracking, and monitoring dynamic progresses of biological activities over a long period.[66]

Tissue regeneration is one of the common processes in living organisms.[67] To study this important phenomenon, many vertebrate genetic models have been used for tissue regeneration. Among them, zebrafish and medaka show good regeneration ability and are suitable for living imaging.[68,69] Kwok, Wang, and Tang et al. developed an AIE probe for monitoring the tissue regeneration of medaka.[70] (*Z*)-3-(4-(4-Methylpiperazin-1-yl)phenyl)-2-(4-(pyridin-4-yl)phenyl) acrylonitrile (CSMPP) was synthesized as a new AIE probe (Figure 6a). The AIE characteristics could be observed in acetonitrile/water mixtures, and the enhanced emission also appeared with the increase of viscosity. In addition, two protonated sites, the *N*-methyl-piperazinyl group and the pyridinyl group, endorsed CSMPP pH-response ability. The fluorescence of CSMPP changed from red to yellow and then to green when the pH increased from 3.45 to 6.80. The response was independent of common chemical species in living systems, such as glucose and natural amino acids. In vitro cell imaging found the targeting ability to the lysosome of CSMPP (Figure 6b). The emission of LysoTracker Red (LTR) and CSMPP overlapped well in costaining experiments, and the Pearson correlation coefficient was 0.92. Moreover, the whole body of the medaka larva could be lit up after feeding with CSMPP for 4 h (Figure 6c). Photostability is also one of the essential requirements for long-term tracking. The good photostability of CSMPP had been confirmed by more than

https://doi.org/10.1021/cbmi.3c00056
Chem. Biomed. Imaging 2023, 1, 509−521

80% fluorescence signals kept after 100 sequential scans. The caudal fin regeneration of the medaka larva was visualized by tracking the pH of the lysosome (Figure 6d). After amputation, the pH decreased and reached a minimum during 24−48 h postamputation (hpa), then increased to an almost normal level when the regeneration progress was about to end (120 hpa). Stimuli-response AIEgens have made a leap from static detection to dynamic monitoring.

Besides the macro life process, microbiological activities could also be tracked by AIEgens. Bacterial invasion is one of the causes of human diseases.[71,72] A study on immunocyte−microbe interactions is significant for the development of antimicrobial methods and medicine.[73] At the early stage of an immune response upon bacterial invasion, the macrophage is the main immunocyte. To visualize the interaction between macrophages with bacteria, Zhao and Tang et al. developed a clickable AIEgen (CDPP-NCS).[74] It had both a targeting group and a click-reactive moiety (Figure 6e). The cationic pyridinium group was able to drive CDPP-NCS to bacteria, and the NCS moiety could combine with amine moieties on the surface of bacteria through a click reaction. The effectiveness of click reaction between CDPP-NCS and amine in biomolecules was confirmed by sodium dodecyl sulfate-polyacrylamide gel electrophoresis (SDS-PAGE), and the great bacteria staining ability was observed with high SNR. Excellent antiphoto bleaching ability had been proven compared to commercial dye FM4−64FX. The bacteria engulfed process by macrophages was visualized by fluorescence imaging (Figure 6f). CDPP-NCS labeled bacteria were ingested by macrophages gradually with no fluorescence escaping to cells, indicating the stability of the covalent coupling between CDPP-NCS and bacteria.

The co-staining experiments were conducted to study the interactions between engulfed bacteria and lysosomes or mitochondria. After CDPP-NCS labeled bacterial and macrophages were incubated for 6 h, the green fluorescence signal from lysosomes overlapped with the red one from bacteria, indicating that phagosomes containing engulfed bacteria will fuse with lysosomes (Figure 6g). On the other hand, the green fluorescence signal from mitochondria gradually moved close to the red one (bacterial), which verified the theory that mitochondria would approach phagosomes to deliver reactive oxygen species (ROS) (Figure 6h).[75] AIEgens work as powerful tools for the interaction among cells, bacteria, fungi, and viruses.

Cell populations are combined with various cells to conduct biological activities as a coordinated system. Many studies about living cell populations were based on in vitro cell culture.[76] However, an *in vitro* cell study could not reveal the real information in vivo since cells have been separated from a complex natural environment, which is difficult to achieve artificially. Fluorescence can visualize real-time cell activities during biological processes in vivo.[77] For example, Zheng and Tang et al. developed an AIEgen (TPE-PyN$_3$) for real-time imaging of cell behaviors.[78] The pyridinium group enabled TPE-PyN$_3$ to target mitochondria (Figure 7a). The mitochondria in cultured cells could be lit up after incubating with TPE-PyN$_3$ for only 5 min with a higher SNR compared to MitoTracker red (MTR) for 15 min (a commercial dye; Figure 7b). The potential for long-term tracking was confirmed by comparing it with a commercial dye 5-chloromethylfluorescein diacetate (CMFDA). The fluorescence of TPE-PyN$_3$ in living cells could remain for multiple generations (Figure 7c). In

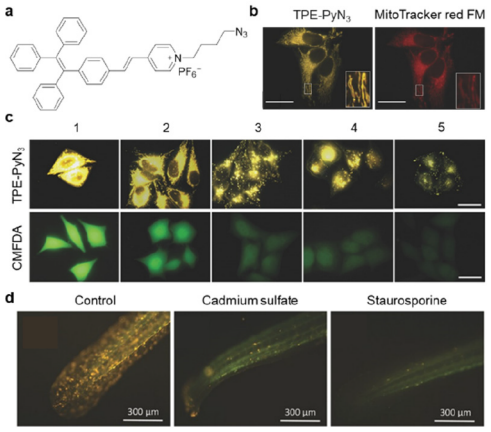

Figure 7. (a) Molecule structure of TPE-PyN3. (b) Merged image of HeLa cells stained with TPE-PyN$_3$ and MitoTracker red FM; scale bar is 30 μm. (c) Fluorescent images of TPE-PyN3 or CellTracker Green CMFDA-stained HeLa cells at various passages; scale bar is 30 μm. (d) Tail rudiment of a living zebrafish embryo stained with TPE-PyN3 in different groups; scale bar is 300 μm. Reproduced with permission from ref 78. Copyright 2016 Wiley-VCH.

living zebrafish embryos, the surface of the whole embryo could be stained by TPE-PyN$_3$ and the fluorescence could be retained for as long as 60 h under physiological conditions. The long-term tracking of cell apoptosis was achieved in living zebrafish. Cadmium sulfate and staurosporine are two agents which could cause cell apoptosis. After being treated with these two drugs, the fluorescence in TPE-PyN$_3$ stained zebrafish almost disappeared (Figure 7d), indicating the onset of apoptosis, when the membrane potential of mitochondrial decrease led to the escape of TPE-PyN$_3$ from mitochondrial.

5. NIR IMAGING

The fluorescent dyes whose emission wavelength usually locate in the visible light region are limited by background autofluorescence of biomolecules, poor tissue penetration, and biological photodamage.[79] Fluorescent materials with NIR emission, especially the NIR-II emission (1000−1700 nm), can avoid autofluorescence interference, deepen imaging depth, and minimize energy loss.[80] Quantum dots and carbon dots have been used as NIR fluorescence probes for in vivo imaging. However, they encounter several common weaknesses, such as high cytotoxicity, obvious photobleaching, and low cellular retention. In addition, organic molecules with NIR emission usually require a large conjugate structure, which indicates easy ACQ and low brightness.[81] NIR AIEgens stand out from them, with high brightness and biocompatibility. Many molecules in the aggregate state could make emissions more stable and brighter. Characteristics of small organic molecules make them low cytotoxicity and excellent cellular retention.[82]

The brain is the control center of biological activities, also related to multiple diseases like Alzheimer's disease and Parkinson's disease.[83,84] As the fundamental of study on brain structure, brain imaging is obviously significant.[85] NIR light, which could image brain structure in depth with its great tissue penetration, has achieved fruitful achievement.[79,80] To construct AIEgens with NIR emission for brain imaging, D-A structures are widely used and could extend the emission wavelength of organic molecules. Tang and Qian et al. designed a NIR emission AIEgen DCBT (Figure 8a) with three-photon fluorescence (3PF) characteristics, which could

https://doi.org/10.1021/cbmi.3c00056
Chem. Biomed. Imaging 2023, 1, 509−521

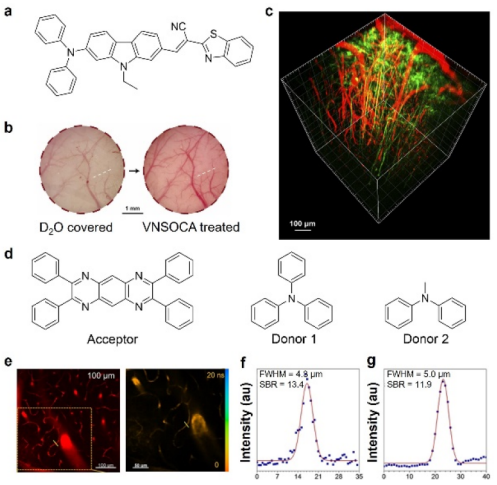

Figure 8. (a) Molecule structure of DCBT. (b) Typical bright field pictures of the mouse brain vasculature before and after skull clearing; scale bar is 1 mm. (c) Reconstructed 3D imaging of the neuron-vessel dual channel from 0 to 600 μm depth; scale bar is 100 μm. Reproduced with permission from ref 86. Copyright 2022 Elsevier. (d) Molecule structure of acceptor, donor 1, and donor 2. (e) Two-photon fluorescence image (left) and fluorescence lifetime image (right) of mouse brain−blood vessels at a depth of 100 μm; scale bar is 100 and 50 μm. (f,g) Plots of pixel intensity across the capillaries (marked with a yellow line) in the image of (e); horizontal coordinates: position (μm). Reproduced with permission from ref 89. Copyright 2022 Wiley-VCH.

be excited by long-wavelength excitation light with low tissue scattering.[86] The mouse skull, which is the protection of the cortex, shows strong scattering. Compared to other technologies applied to avoid scattering of skulls, in vivo skull optical clearing (SOC) technique, which could create a transparent window by using several chemical agents in the skulls of mice, is safer and more repeatable.[87] To avoid absorption of H_2O in the NIR region, the authors used D_2O as a substitute (Figure 8b). The 3PF imaging of brain vasculature could reach 1000 μm after SOC treatment. Neurons at the neocortex layers were also imaged at a depth of 600 μm (Figure 8c).

The D-A structure could red-shift the emission by strong intramolecular charge transfer (ICT). In addition, through-space charge transfer, which occurs in the complexes of donors and acceptors, could also induce the red-shift of emission.[88] Qian, Chen, and Tang et al. achieved NIR emission by simply encapsulating acceptors and donors in nanoparticles (NPs).[89] 2,3,7,8-Tetraphenylpyrazino[2, 3-g]quinoxaline was chosen as the acceptor, at the same time, TPA and *N*-methyl-*N*-phenylaniline were selected as two different donors (Figure 8d). The obtained complexes showed excellent two-photon NIR fluorescence. Theory calculation results showed an obvious through-space charge transfer between donors and acceptors. The twisted conformation of donors and acceptors induced weak $\pi\cdots\pi$ stacking, which is the cause of ACQ. Both fluorescence imaging and fluorescence lifetime imaging could be observed with high resolution and good contrast using the NPs (Figure 8e). Capillaries are clearly visible in the NIR images. Similar blood vessel widths were measured as 4.3 and 4.7 μm separately (Figure 8f, g), indicating uniform morphology of the capillaries in brain tissue. Bright emission promises AIEgens great imaging ability in deep tissue in the NIR region.

Chemiluminescence (CL) imaging can avoid autofluorescence interference and photodamage caused by thermal effects without using excitation light. High SNR has been achieved in imaging immunoassays and tumors using CL.[90,91] In vivo NIR-II imaging was greatly improved through CL, which could be accomplished by cascade chemiluminescence resonance energy transfer (CRET) and Förster resonance energy transfer (FRET). Fan and Zhang et al. encapsulated chemiluminogens and two AIEgens, which possess overlapped emission and absorption regions, in nanoparticles to construct a cascade CRET and FRET system.[92] Once encountered with ROS, the CLgens would be excited and transfer energy to BTD540 (red emission) and then to BBTD700 (NIR-II emission). They realized high-contrast NIR-II imaging of immunoassays, compared with fluorescence, on living mice by using this system. Zhang and Tang et al. greatly improved the quantum yields (QYs) of NIR-II PL and CL by adjusting the donor of AIEgens (Figure 9a).[93] TPE-BBT exhibited a higher QY than

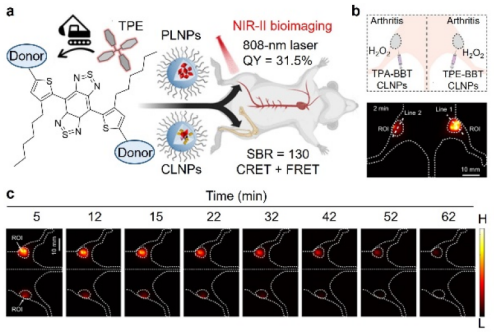

Figure 9. (a) Schematic illustration of strategies for NIR-II bioimaging. (b) Schematic illustration of chemiluminescence imaging of the arthrosis in mice (up) and in vivo NIR-II CL imaging using 0.66 mg of TPE-BBT (line 1) and TPA-BBT (line 2) CLNPs after injection for 2 min (down); scale bar is 10 mm. (c) In vivo NIR-II CL imaging of TPE-BBT (up) and TPA-BBT (down) CLNPs of arthrosis inflammation at different postinjection times, respectively. Scale bar: 10 mm. Reproduced with permission from ref 93. Copyright 2022 American Chemical Society.

TPA-BBT in the crystalline state, as a result of its stronger intermolecular interactions. Calculation results also show the weaker electron-donating ability of the TPE moiety than that of the TPA moiety, indicating the reduction of the dark TICT effect and increase of QY. The PLNPs of TPE-BBT performed well for blood vessel imaging, with the highest signal-to-background ratio (SBR) compared with TPA-BBT and indocyanine green (ICG). The performances of TPE-BBT and TPA-BBT for arthrosis inflammation imaging were observed in CLNPs. TPE-BBT CLNPs showed higher CL intensity after the injection for 2 min (Figure 9b). TPA-BBT CLNPs show good imaging ability for long-term tracking. On the other hand, higher quality CL imaging of TPE-BBT was observed, which could persist for even 62 min with an SBR larger than 10 (Figure 9c). CL AIEgens enable further improvement in the clarity and contrast of the NIR imaging.

6. SUMMARY AND OUTLOOK

In the last two decades, we have witnessed a boom in the number and structural diversities of AIEgens developed by scientists around the world.[94] The emission wavelength of AIEgens covered the full visible wavelength range and further

https://doi.org/10.1021/cbmi.3c00056
Chem. Biomed. Imaging 2023, 1, 509−521

Scheme 2. Scale of AIE Bioimaging[a]

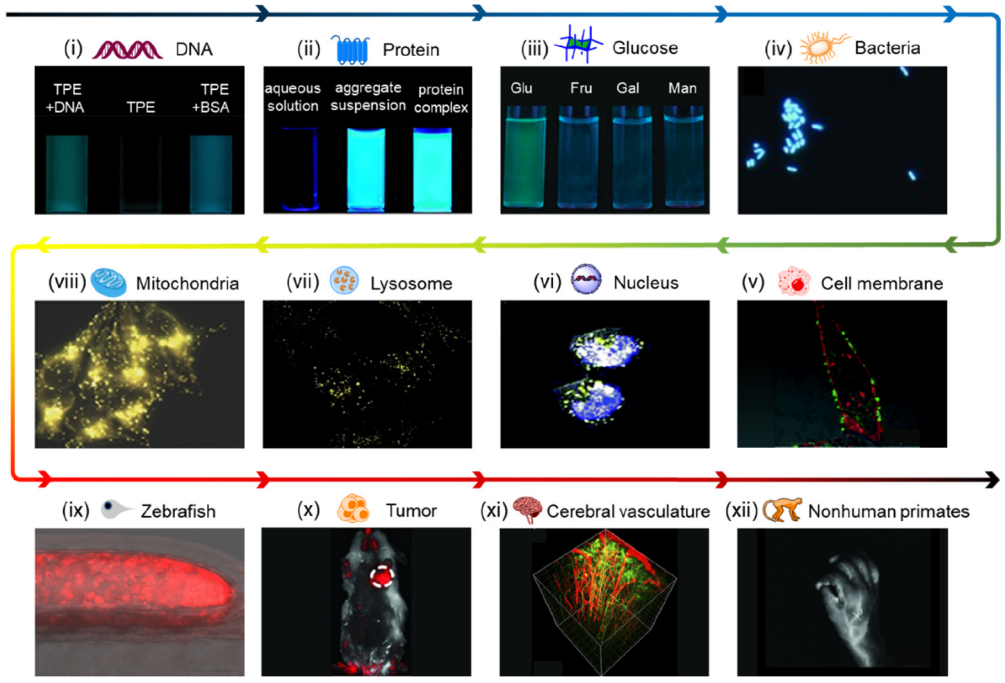

[a](i) Detection of DNA. Reproduced with permission from ref 95. Copyright 2006 Royal Society of Chemistry. (ii) Detection of protein. Reproduced with permission from ref 96. Copyright 2007 American Chemical Society. (iii) Detection of glucose. Reproduced with permission from ref 97. Copyright 2011 American Chemical Society. (iv) Detection of bacteria. Reproduced with permission from ref 98. Copyright 2014 WILEY-VCH. (v) Imaging of cell membrane. Reproduced with permission from ref 99. Copyright 2019 Royal Society of Chemistry. (vi) Imaging of nucleus. Reproduced with permission from ref 100. Copyright 2017 Royal Society of Chemistry. (vii) Imaging of lysosome. Reproduced with permission from ref 101. Copyright 2021 Springer Nature. (viii) Imaging of mitochondria. Reproduced with permission from ref 102. Copyright 2016 WILEY-VCH. (ix) Imaging of zebrafish. Reproduced with permission from ref 28. Copyright 2022 American Chemical Society. (x) Imaging of tumor. Reproduced with permission from ref 103. Copyright 2012 WILEY-VCH. (xi) Imaging of cerebral vasculature. Reproduced with permission from ref 104. Copyright 2017 WILEY-VCH. (xii) Imaging of nonhuman primates. Reproduced with permission from ref 105. Copyright 2020 American Association for the Advancement of Science.

extended to the NIR region in bioimaging. AIEgens have been successfully applied at different levels, from biomolecule detection to organelle-targeted cell imaging, from live imaging of small animals to senior primates (Scheme 2). This Review summarizes recent progress on various types of AIEgens for bioimaging, including turn-on imaging, stimuli-response sensing, long-term tracking, and NIR imaging. The advantages of AIEgens in the field of bioimaging are summarized:[1] AIEgens show prominent turn-on characteristics in the physiological environment since the change from a single molecule state to the aggregate state;[2] high brightness and anti-photobleaching ability in the aggregate state endow AIEgens with excellent SNR and potential for long-time imaging;[3] various emission colors and responses to different stimuli can be achieved by adjusting the molecular structure.

Despite numerous achievements in the field of bioimaging, there are several possible new opportunities to be explored:[1] Besides bright fluorescence, room temperature phosphorescence (RTP) could also be achieved in AIEgens. Most of the aggregation-induced phosphorescence luminogens (AIPgens) with RTP characteristics were developed for emergency lighting and anticounterfeiting, but very few were applied for bioimaging.[106] The long emission lifetime of RTP materials enables stable afterglow signals, which provide possibilities to avoid autofluorescence of organisms and achieve high-quality bioimaging.[2] Some AIEgens can generate ROS upon irradiation, which would further trigger some biological activities like apoptosis. However, detection of the ROS-triggered process is still unexplored. Therefore, it is of great interest to develop new AIEgens which can generate ROS and simultaneously track the subsequent biological processes.[3] Some AIEgens have been commercialized for bioimaging, yet clinical applications still have a long way to go due to biosafety issues.[107] On the other hand, several examples of vessel imaging of nonhuman primates have been reported as a first step toward clinical diagnosis and surgical navigation in the future.[105]

AUTHOR INFORMATION

Corresponding Authors

Zijie Qiu − *School of Science and Engineering, Shenzhen Institute of Aggregate Science and Technology, The Chinese University of Hong Kong, Shenzhen, Guangdong 518172, China;* orcid.org/0000-0003-0728-1178; Email: zijieqiu@cuhk.edu.cn

Zheng Zhao − *School of Science and Engineering, Shenzhen Institute of Aggregate Science and Technology, The Chinese University of Hong Kong, Shenzhen, Guangdong 518172, China; HKUST-Shenzhen Research Institute, Shenzhen, Guangdong Province 518057, China;* orcid.org/0000-0002-5536-0439; Email: zhaozheng@cuhk.edu.cn

Ben Zhong Tang − *School of Science and Engineering, Shenzhen Institute of Aggregate Science and Technology, The Chinese University of Hong Kong, Shenzhen, Guangdong*

https://doi.org/10.1021/cbmi.3c00056
Chem. Biomed. Imaging 2023, 1, 509−521

518172, China; AIE Institute, Huangpu, Guangdong 510530, China; Department of Chemistry, Hong Kong Branch of Chinese National Engineering Research Center for Tissue Restoration and Reconstruction, The Hong Kong University of Science and Technology, Kowloon, Hong Kong, China; orcid.org/0000-0002-0293-964X; Email: tangbenz@cuhk.edu.cn

Authors

Siyuan Wang − *School of Science and Engineering, Shenzhen Institute of Aggregate Science and Technology, The Chinese University of Hong Kong, Shenzhen, Guangdong 518172, China*

Kun Zhou − *School of Science and Engineering, Shenzhen Institute of Aggregate Science and Technology, The Chinese University of Hong Kong, Shenzhen, Guangdong 518172, China*

Xinyan Lyu − *School of Science and Engineering, Shenzhen Institute of Aggregate Science and Technology, The Chinese University of Hong Kong, Shenzhen, Guangdong 518172, China*

Haowen Li − *School of Science and Engineering, Shenzhen Institute of Aggregate Science and Technology, The Chinese University of Hong Kong, Shenzhen, Guangdong 518172, China*

Complete contact information is available at: https://pubs.acs.org/10.1021/cbmi.3c00056

Author Contributions

#S.W. and K.Z. contributed equally to this work.

Notes

The authors declare no competing financial interest.

■ ACKNOWLEDGMENTS

This work is financially supported by the National Natural Science Foundation of China (52003228, 52273197, and 21788102), Shenzhen Key Laboratory of Functional Aggregate Materials (ZDSYS20211021111400001), the Science, Technology and Innovation Commission of Shenzhen Municipality (JCYJ20220818103007014, JCYJ20213241346130 38, JCYJ20220530143805012, KQTD20210811090142053, JSGG20220606141800001, GJHZ20210705141810031), the China Postdoctoral Science Foundation (2022M713022), the Open Fund of Guangdong Provincial Key Laboratory of Luminescence from Molecular Aggregates (2021-kllma-08), Guangzhou 510640, China (South China University of Technology), and Guangdong Basic and Applied Basic Research Foundation (2023A1515011342).

■ LIST OF ABBREVIATIONS

ACQ	Aggregation-caused quenching
AIE	Aggregation-induced emission
AIEgen	Aggregate-induced emission luminogen
AIPgen	Aggregation-induced phosphorescence luminogen
BG	*O*6-benzylguanine
BODIPY	Boron dipyrromethene
BSM	Benzothiadiazol-7-ylidene malononitrile
CK	Creatine kinase
CL	Chemiluminescence
CMFDA	5-Chloromethylfluorescein diacetate
COTh	Cyclooctatetrathiophene
CRET	Chemiluminescence resonance energy transfer
CSMPP	(*Z*)-3-(4-(4-Methylpiperazin-1-yl) phenyl)-2-(4-(pyridin-4-yl) phenyl) acrylonitrile
CTE	Clustering-triggered emission
DFT	Density functional theory
DMSO	Dimethyl sulfoxide
DNFB	1-Fluoro-2,4-dinitrobenzene
E. coli	*Escherichia coli*
FRET	Förster resonance energy transfer
hpa	Hours postamputation
ICT	Intramolecular charge transfer
LD	Lipid droplet
LPS	Lipopolysaccharide
LTG	Lysotracker Green
LTR	Lysotracker Red
MD	Molecular dynamics
MRSA	Methicillin-resistant *Staphylococcus aureus*
MTG	Mitotracker Green
MTR	Mitotracker red
NIR	Near-infrared
NP	Nanoparticle
PBS	Phosphate-buffered saline
PNVCL	Poly(*N*-vinylcaprolactam)
QY	Quantum yield
RIM	Restriction of intramolecular motion
RIR	Restriction of intramolecular rotation
RIV	Restriction of intramolecular vibration
ROS	Reactive oxygen species
RTP	Room temperature phosphorescence
SBR	Signal-to-background ratio
SNR	Signal-to-noise ratios
SOC	Skull optical clearing
TD-DFT	Time-dependent density functional theory
TICT	Twisted intramolecular charge transfer
TPA	Triphenylamine
TPE	Tetraphenylethylene

■ VOCABULARY

Aggregation-induced emission: fluorescence molecule achieves the change from no-emission to bright emission through aggregation process

Visualization: use of a strategy to make things that cannot be seen directly by the naked eye visible

Turn-on imaging: strategies for achieving luminescence turn-on in organisms

Stimuli-response sensing: environmental detection through response to stimuli

Long-term tracking: monitoring of biobehavior for a long time

NIR imaging: imaging using near-infrared fluorescence

■ REFERENCES

(1) Bardell, D. The Biologists' Forum: The Invention of the Microscope. *BIOS* **2004**, *75*, 78.

(2) Reynaud, E. G. The Biology of Imaging. *Philos. Trans. R. Soc. A* **2022**, *380*, 20200389.

(3) Kriss, T. C.; Kriss, V. M. History of the Operating Microscope: From Magnifying Glass to Microneurosurgery. *Neurosurg.* **1998**, *42*, 899.

(4) Lin, M. T.; Beal, M. F. Mitochondrial Dysfunction and Oxidative Stress in Neurodegenerative Diseases. *Nature* **2006**, *443*, 787.

(5) McFadden, G. I. Endosymbiosis and Evolution of the Plant Cell. *Curr. Opin. Plant Biol.* **1999**, *2*, 513.

(6) Ellis, J. Observations on a Particular Manner of Increase in the Animalcula of Vegetable Infusions, with the Discovery of an

Indissoluble Salt Arising from Hemp-Seed Put into Water Till It Becomes Putrid. *Philos. Trans. R. Soc.* **1769**, *59*, 138.
(7) Stokes, G. G. On the Change of Refrangibility of Light. *Philos. Trans. R. Soc.* **1852**, *142*, 463.
(8) Renz, M. Fluorescence Microscopy-a Historical and Technical Perspective. *Cytometry A* **2013**, *83*, 767.
(9) Lou, X.; Zhao, Z.; Tang, B. Z. Organic Dots Based on Aiegens for Two-Photon Fluorescence Bioimaging. *Small* **2016**, *12*, 6430.
(10) Ma, Y.; Chen, Q.; Pan, X.; Zhang, J. Insight into Fluorescence Imaging and Bioorthogonal Reactions in Biological Analysis. *Top. Curr. Chem.* **2021**, *379*, 10.
(11) Chang, H.; Karan, N. S.; Shin, K.; Bootharaju, M. S.; Nah, S.; Chae, S. I.; Baek, W.; Lee, S.; Kim, J.; Son, Y. J.; Kang, T.; Ko, G.; Kwon, S. H.; Hyeon, T. Highly Fluorescent Gold Cluster Assembly. *J. Am. Chem. Soc.* **2021**, *143*, 326.
(12) Yang, T. Q.; Peng, B.; Shan, B. Q.; Zong, Y. X.; Jiang, J. G.; Wu, P.; Zhang, K. Origin of the Photoluminescence of Metal Nanoclusters: From Metal-Centered Emission to Ligand-Centered Emission. *Nanomater.* **2020**, *10*, 261.
(13) Meng, T.; Zheng, Y.; Zhao, D.; Hu, H.; Zhu, Y.; Xu, Z.; Ju, S.; Jing, J.; Chen, X.; Gao, H.; Yang, K.; Guo, T.; Li, F.; Fan, J.; Qian, L. Ultrahigh-Resolution Quantum-Dot Light-Emitting Diodes. *Nat. Photonics* **2022**, *16*, 297.
(14) Tseng, Z.-L.; Chen, L.-C.; Chao, L.-W.; Tsai, M.-J.; Luo, D.; Al Amin, N. R.; Liu, S.-W.; Wong, K.-T. Aggregation Control, Surface Passivation, and Optimization of Device Structure toward near-Infrared Perovskite Quantum-Dot Light-Emitting Diodes with an Eqe up to 15.4%. *Adv. Mater.* **2022**, *34*, 2109785.
(15) Wang, B.; Lu, S. The Light of Carbon Dots: From Mechanism to Applications. *Matter* **2022**, *5*, 110.
(16) Li, J.; Gong, X. The Emerging Development of Multicolor Carbon Dots. *Small* **2022**, *18*, 2205099.
(17) Chua, M. H.; Chin, K. L. O.; Loh, X. J.; Zhu, Q.; Xu, J. Aggregation-Induced Emission-Active Nanostructures: Beyond Biomedical Applications. *ACS Nano* **2023**, *17*, 1845.
(18) Luo, J.; Xie, Z.; Lam, J. W.; Cheng, L.; Chen, H.; Qiu, C.; Kwok, H. S.; Zhan, X.; Liu, Y.; Zhu, D.; Tang, B. Z. Aggregation-Induced Emission of 1-Methyl-1,2,3,4,5-Pentaphenylsilole. *Chem. Commun.* **2001**, *18*, 1740.
(19) Zhao, Z.; Zhang, H.; Lam, J. W. Y.; Tang, B. Z. Aggregation-Induced Emission: New Vistas at the Aggregate Level. *Angew. Chem., Int. Ed.* **2020**, *59*, 9888.
(20) Xu, S.; Duan, Y.; Liu, B. Precise Molecular Design for High-Performance Luminogens with Aggregation-Induced Emission. *Adv. Mater.* **2020**, *32*, 1903530.
(21) Zhao, Z.; Chen, C.; Wu, W.; Wang, F.; Du, L.; Zhang, X.; Xiong, Y.; He, X.; Cai, Y.; Kwok, R. T. K.; Lam, J. W. Y.; Gao, X.; Sun, P.; Phillips, D. L.; Ding, D.; Tang, B. Z. Highly Efficient Photothermal Nanoagent Achieved by Harvesting Energy via Excited-State Intramolecular Motion within Nanoparticles. *Nat. Commun.* **2019**, *10*, 768.
(22) Liao, Y.; Li, B.; Zhao, Z.; Fu, Y.; Tan, Q.; Li, X.; Wang, W.; Yin, J.; Shan, H.; Tang, B. Z.; Huang, X. Targeted Theranostics for Tuberculosis: A Rifampicin-Loaded Aggregation-Induced Emission Carrier for Granulomas Tracking and Anti-Infection. *ACS Nano* **2020**, *14*, 8046.
(23) Wu, Q.; Li, Y.; Wang, L.; Wang, D.; Tang, B. Z. Aggregation-Induced Emission: An Emerging Concept in Brain Science. *Biomaterials* **2022**, *286*, 121581.
(24) Shi, J.; Zhang, S.; Zheng, M.; Deng, Q.; Zheng, C.; Li, J.; Huang, F. A Novel Fluorometric Turn-on Assay for Lipase Activity Based on an Aggregation-Induced Emission (AIE) Luminogen. *Sens. Actuators B Chem.* **2017**, *238*, 765.
(25) Gong, S.; Qin, A.; Zhang, Y.; Li, M.; Chen, X.; Liang, Y.; Xu, X.; Wang, Z.; Wang, S. A New Ratiometric AIE Fluorescent Probe for Detecting Cysteine in Food Samples and Imaging in the Biological System. *Food Chem.* **2023**, *400*, 134108.
(26) Zhu, C.; Kwok, R. T. K.; Lam, J. W. Y.; Tang, B. Z. Aggregation-Induced Emission: A Trailblazing Journey to the Field of Biomedicine. *ACS Appl. Bio. Mater.* **2018**, *1*, 1768.
(27) Zhao, Z.; Zheng, X.; Du, L.; Xiong, Y.; He, W.; Gao, X.; Li, C.; Liu, Y.; Xu, B.; Zhang, J.; Song, F.; Yu, Y.; Zhao, X.; Cai, Y.; He, X.; Kwok, R. T. K.; Lam, J. W. Y.; Huang, X.; Lee Phillips, D.; Wang, H.; Tang, B. Z. Non-Aromatic Annulene-Based Aggregation-Induced Emission System via Aromaticity Reversal Process. *Nat. Commun.* **2019**, *10*, 2952.
(28) Yu, Y.; Xing, H.; Park, H.; Zhang, R.; Peng, C.; Sung, H. H. Y.; Williams, I. D.; Ma, C.; Wong, K. S.; Li, S.; Xiong, Q.; Li, M.-H.; Zhao, Z.; Tang, B. Z. Deep-Red Aggregation-Induced Emission Luminogen Based on Dithiofuvalene-Fused Benzothiadiazole for Lipid Droplet-Specific Imaging. *ACS Mater. Lett.* **2022**, *4*, 159.
(29) Zhao, N.; Li, Y.; Yang, W.; Zhuang, J.; Li, Y.; Li, N. Multifunctional Pyrazoline Based Aiegens: Real-Time Tracking and Specific Protein "Fishing" of Lipid Droplets. *Chem. Sci.* **2019**, *10*, 9009.
(30) Halbach, K.; Ulrich, N.; Goss, K.-U.; Seiwert, B.; Wagner, S.; Scholz, S.; Luckenbach, T.; Bauer, C.; Schweiger, N.; Reemtsma, T. Yolk Sac of Zebrafish Embryos as Backpack for Chemicals? *Environ. Sci. Technol.* **2020**, *54*, 10159.
(31) Zang, T.; Xie, Y.; Su, S.; Liu, F.; Chen, Q.; Jing, J.; Zhang, R.; Niu, G.; Zhang, X. In Vitro Light-up Visualization of a Subunit-Specific Enzyme by an AIE Probe via Restriction of Single Molecular Motion. *Angew. Chem., Int. Ed.* **2020**, *59*, 10003.
(32) Hanaoka, K.; Iwaki, S.; Yagi, K.; Myochin, T.; Ikeno, T.; Ohno, H.; Sasaki, E.; Komatsu, T.; Ueno, T.; Uchigashima, M.; Mikuni, T.; Tainaka, K.; Tahara, S.; Takeuchi, S.; Tahara, T.; Uchiyama, M.; Nagano, T.; Urano, Y. General Design Strategy to Precisely Control the Emission of Fluorophores via a Twisted Intramolecular Charge Transfer (Tict) Process. *J. Am. Chem. Soc.* **2022**, *144*, 19778.
(33) Grabowski, Z. R.; Rotkiewicz, K.; Rettig, W. Structural Changes Accompanying Intramolecular Electron Transfer: Focus on Twisted Intramolecular Charge-Transfer States and Structures. *Chem. Rev.* **2003**, *103*, 3899.
(34) Popa, I.; Berkovich, R.; Alegre-Cebollada, J.; Badilla, C. L.; Rivas-Pardo, J. A.; Taniguchi, Y.; Kawakami, M.; Fernandez, J. M. Nanomechanics of Halotag Tethers. *J. Am. Chem. Soc.* **2013**, *135*, 12762.
(35) Gautier, A.; Juillerat, A.; Heinis, C.; Corrêa, I. R.; Kindermann, M.; Beaufils, F.; Johnsson, K. An Engineered Protein Tag for Multiprotein Labeling in Living Cells. *Chem. Biol.* **2008**, *15*, 128.
(36) Zhou, Y.; Hua, J.; Tang, B. Z.; Tang, Y. Aiegens in Cell-Based Multiplex Fluorescence Imaging. *Sci. China Chem.* **2019**, *62*, 1312.
(37) Huang, X.; Zhang, R.; Chen, C.; Kwok, R. T. K.; Tang, B. Z. Wash-Free Detection and Bioimaging by Aiegens. *Mater. Chem. Front.* **2021**, *5*, 723.
(38) Zhang, J.; He, B.; Hu, Y.; Alam, P.; Zhang, H.; Lam, J. W. Y.; Tang, B. Z. Stimuli-Responsive Aiegens. *Adv. Mater.* **2021**, *33*, 2008071.
(39) Ellenbroek, S. I. J.; Iden, S.; Collard, J. G. Cell Polarity Proteins and Cancer. *Semin. Cancer Biol.* **2012**, *22*, 208.
(40) Bartholomew, J. W.; Mittwer, T. The Gram Stain. *Bacteriol. Rev.* **1952**, *16*, 1.
(41) Wang, C.; Wang, J.; Xue, K.; Xiao, M.; Wu, K.; Lv, S.; Hao, B.; Zhu, C. Polarity-Sensitive Fluorescent Probe for Reflecting the Packing Degree of Bacterial Membrane Lipids. *Anal. Chem.* **2022**, *94*, 3303.
(42) Li, H.; Shi, W.; Li, X.; Hu, Y.; Fang, Y.; Ma, H. Ferroptosis Accompanied by •OH Generation and Cytoplasmic Viscosity Increase Revealed via Dual-Functional Fluorescence Probe. *J. Am. Chem. Soc.* **2019**, *141*, 18301.
(43) Zhai, S.; Hu, W.; Wang, W.; Chai, L.; An, Q.; Li, C.; Liu, Z. Tracking Autophagy Process with a through Bond Energy Transfer-Based Ratiometric Two-Photon Viscosity Probe. *Biosens. Bioelectron.* **2022**, *213*, 114484.
(44) Wu, W.-N.; Song, Y.-F.; Zhao, X.-L.; Wang, Y.; Fan, Y.-C.; Xu, Z.-H.; James, T. D. Multifunctional 1,3-Benzoxazole-Merocyanine-Based Probe for the Ratiometric Fluorescence Detection of Ph /Hso3- /Viscosity in Mitochondria. *Chem. Eng. J.* **2023**, *464*, 142553.

https://doi.org/10.1021/cbmi.3c00056
Chem. Biomed. Imaging 2023, 1, 509−521

(45) Zheng, D.-J.; Yang, Y.-S.; Zhu, H.-L. Recent Progress in the Development of Small-Molecule Fluorescent Probes for the Detection of Hydrogen Peroxide. *Trends Analyt. Chem.* **2019**, *118*, 625.
(46) Yang, X.; Zhang, D.; Ye, Y.; Zhao, Y. Recent Advances in Multifunctional Fluorescent Probes for Viscosity and Analytes. *Coord. Chem. Rev.* **2022**, *453*, 214336.
(47) Wang, X.; Fan, L.; Wang, S.; Zhang, Y.; Li, F.; Zan, Q.; Lu, W.; Shuang, S.; Dong, C. Real-Time Monitoring Mitochondrial Viscosity During Mitophagy Using a Mitochondria-Immobilized near-Infrared Aggregation-Induced Emission Probe. *Anal. Chem.* **2021**, *93*, 3241.
(48) Su, S.; Chai, L.; An, Q.; Hu, W.; Wang, L.; Li, X.; Zhang, H.; Li, C. Tracking Autophagy Process with a Tbet and AIE-Based Ratiometric Two-Photon Viscosity Probe. *Anal. Chem.* **2022**, *94*, 15146.
(49) Feng, Y.; Nie, G.; Liang, W.; Li, W.; Zhang, Y.; Wang, K.; Chen, D. Real-Time Imaging of Acute Alcoholic Liver Injury in Vivo via a Robust Viscosity Probe with Aggregation-Induced Emission Nature. *Sens. Actuators B Chem.* **2022**, *355*, 131285.
(50) Shi, W. J.; Chen, R.; Yang, J.; Wei, Y. F.; Guo, Y.; Wang, Z. Z.; Yan, J. W.; Niu, L. Novel Meso-Benzothiazole-Substituted Bodipy-Based AIE Fluorescent Rotor for Imaging Lysosomal Viscosity and Monitoring Autophagy. *Anal. Chem.* **2022**, *94*, 14707.
(51) Yu, C.; Huang, Z.; Gu, W.; Wu, Q.; Hao, E.; Xiao, Y.; Jiao, L.; Wong, W.-Y. A Novel Family of AIE-Active Meso-2-Ketopyrrolyl Bodipys: Bright Solid-State Red Fluorescence, Morphological Properties and Application as Viscosimeters in Live Cells. *Mater. Chem. Front.* **2019**, *3*, 1823.
(52) Shi, W.-J.; Yang, J.; Wei, Y.-F.; Li, X.-T.; Yan, X.-H.; Wang, Y.; Leng, H.; Zheng, L.; Yan, J.-w. Novel Cationic Meso-Cf3 Bodipy-Based AIE Fluorescent Rotors for Imaging Viscosity in Mitochondria. *Chem. Commun.* **2022**, *58*, 1930.
(53) Edinger, A. L.; Thompson, C. B. Death by Design: Apoptosis, Necrosis and Autophagy. *Curr. Opin. Cell Biol.* **2004**, *16*, 663.
(54) Park, H. J.; Lim, C. S.; Kim, E. S.; Han, J. H.; Lee, T. H.; Chun, H. J.; Cho, B. R. Measurement of Ph Values in Human Tissues by Two-Photon Microscopy. *Angew. Chem., Int. Ed.* **2012**, *51*, 2673.
(55) Yu, F.; Jing, X.; Lin, W. Single-/Dual-Responsive Ph Fluorescent Probes Based on the Hybridization of Unconventional Fluorescence and Fluorophore for Imaging Lysosomal Ph Changes in HeLa Cells. *Anal. Chem.* **2019**, *91*, 15213.
(56) Chen, G.; Fu, Q.; Yu, F.; Ren, R.; Liu, Y.; Cao, Z.; Li, G.; Zhao, X.; Chen, L.; Wang, H.; You, J. Wide-Acidity-Range Ph Fluorescence Probes for Evaluation of Acidification in Mitochondria and Digestive Tract Mucosa. *Anal. Chem.* **2017**, *89*, 8509.
(57) Gu, Y.; Zhao, Z.; Niu, G.; Zhang, H.; Wang, Y.; Kwok, R. T. K.; Lam, J. W. Y.; Tang, B. Z. Visualizing Semipermeability of the Cell Membrane Using a Ph-Responsive Ratiometric Aiegen. *Chem. Sci.* **2020**, *11*, 5753.
(58) Warner, D. A.; Shine, R. The Adaptive Significance of Temperature-Dependent Sex Determination in a Reptile. *Nature* **2008**, *451*, 566.
(59) Hiruta, Y.; Shimamura, M.; Matsuura, M.; Maekawa, Y.; Funatsu, T.; Suzuki, Y.; Ayano, E.; Okano, T.; Kanazawa, H. Temperature-Responsive Fluorescence Polymer Probes with Accurate Thermally Controlled Cellular Uptakes. *ACS Macro Lett.* **2014**, *3*, 281.
(60) Yang, J.; Gu, K.; Shi, C.; Li, M.; Zhao, P.; Zhu, W.-H. Fluorescent Thermometer Based on a Quinolinemalononitrile Copolymer with Aggregation-Induced Emission Characteristics. *Mater. Chem. Front.* **2019**, *3*, 1503.
(61) Zhao, Y.; Wu, Y.; Chen, S.; Deng, H.; Zhu, X. Building Single-Color AIE-Active Reversible Micelles to Interpret Temperature and Ph Stimuli in Both Solutions and Cells. *Macromolecules* **2018**, *51*, 5234.
(62) Saha, B.; Ruidas, B.; Mete, S.; Mukhopadhyay, C. D.; Bauri, K.; De, P. AIE-Active Non-Conjugated Poly(N-Vinylcaprolactam) as a Fluorescent Thermometer for Intracellular Temperature Imaging. *Chem. Sci.* **2020**, *11*, 141.
(63) Zhou, X.; Luo, W.; Nie, H.; Xu, L.; Hu, R.; Zhao, Z.; Qin, A.; Tang, B. Z. Oligo(Maleic Anhydride) S: A Platform for Unveiling the Mechanism of Clusteroluminescence of Non-Aromatic Polymers. *J. Mater. Chem. C* **2017**, *5*, 4775.
(64) Chu, B.; Zhang, H.; Chen, K.; Liu, B.; Yu, Q.-L.; Zhang, C.-J.; Sun, J.; Yang, Q.; Zhang, X.-H.; Tang, B. Z. Aliphatic Polyesters with White-Light Clusteroluminescence. *J. Am. Chem. Soc.* **2022**, *144*, 15286.
(65) Ding, D.; Mao, D.; Li, K.; Wang, X.; Qin, W.; Liu, R.; Chiam, D. S.; Tomczak, N.; Yang, Z.; Tang, B. Z.; Kong, D.; Liu, B. Precise and Long-Term Tracking of Adipose-Derived Stem Cells and Their Regenerative Capacity via Superb Bright and Stable Organic Nanodots. *ACS Nano* **2014**, *8*, 12620.
(66) Huang, L.; Qing, D.; Zhao, S.; Wu, X.; Yang, K.; Ren, X.; Zheng, X.; Lan, M.; Ye, J.; Zeng, L.; Niu, G. Acceptor-Donor-Acceptor Structured Deep-Red AIE Photosensitizer: Lysosome-Specific Targeting, in Vivo Long-Term Imaging, and Effective Photodynamic Therapy. *Chem. Eng. J.* **2022**, *430*, 132638.
(67) Tanaka, E. M. Regenerating Tissues. *Science* **2018**, *360*, 374.
(68) Forbes, S. J.; Rosenthal, N. Preparing the Ground for Tissue Regeneration: From Mechanism to Therapy. *Nat. Med.* **2014**, *20*, 857.
(69) Takayama, K.; Muto, A.; Kikuchi, Y. Leucine/Glutamine and V-Atpase/Lysosomal Acidification via Mtorc1 Activation Are Required for Position-Dependent Regeneration. *Sci. Rep.* **2018**, *8*, 8278.
(70) Shi, X.; Yan, N.; Niu, G.; Sung, S. H. P.; Liu, Z.; Liu, J.; Kwok, R. T. K.; Lam, J. W. Y.; Wang, W. X.; Sung, H. H.; Williams, I. D.; Tang, B. Z. In Vivo Monitoring of Tissue Regeneration Using a Ratiometric Lysosomal AIE Probe. *Chem. Sci.* **2020**, *11*, 3152.
(71) Lam, K. C.; Araya, R. E.; Huang, A.; Chen, Q.; Di Modica, M.; Rodrigues, R. R.; Lopès, A.; Johnson, S. B.; Schwarz, B.; Bohrnsen, E.; Cogdill, A. P.; Bosio, C. M.; Wargo, J. A.; Lee, M. P.; Goldszmid, R. S. Microbiota Triggers Sting-Type I Ifn-Dependent Monocyte Reprogramming of the Tumor Microenvironment. *Cell* **2021**, *184*, 5338.
(72) Belland, R. J.; Ouellette, S. P.; Gieffers, J.; Byrne, G. I. Chlamydia Pneumoniae and Atherosclerosis. *Cell. Microbiol.* **2004**, *6*, 117.
(73) Welte, M. A. Expanding Roles for Lipid Droplets. *Curr. Biol.* **2015**, *25*, R470.
(74) Zhang, Z.; He, W.; Deng, Z.; Liu, Y.; Wen, H.; Wang, Y.; Ye, Z.; Kin Kwok, R. T.; Qiu, Z.; Zhao, Z.; Tang, B. Z. A Clickable Aiegen for Visualization of Macrophage-Microbe Interaction. *Biosens. Bioelectron.* **2022**, *216*, 114614.
(75) Abuaita, B. H.; Schultz, T. L.; O'Riordan, M. X. Mitochondria-Derived Vesicles Deliver Antimicrobial Reactive Oxygen Species to Control Phagosome-Localized Staphylococcus Aureus. *Cell Host Microbe* **2018**, *24*, 625.
(76) Crome, S. Q.; Nguyen, L. T.; Lopez-Verges, S.; Yang, S. Y. C.; Martin, B.; Yam, J. Y.; Johnson, D. J.; Nie, J.; Pniak, M.; Yen, P. H.; Milea, A.; Sowamber, R.; Katz, S. R.; Bernardini, M. Q.; Clarke, B. A.; Shaw, P. A.; Lang, P. A.; Berman, H. K.; Pugh, T. J.; Lanier, L. L.; Ohashi, P. S. A Distinct Innate Lymphoid Cell Population Regulates Tumor-Associated T Cells. *Nat. Med.* **2017**, *23*, 368.
(77) Liang, L.; Liu, C.; Jiao, X.; Zhao, L.; Zeng, X. A Highly Selective and Sensitive Photoinduced Electron Transfer (Pet) Based Hocl Fluorescent Probe in Water and Its Endogenous Imaging in Living Cells. *Chem. Commun.* **2016**, *52*, 7982.
(78) Situ, B.; Chen, S.; Zhao, E.; Leung, C. W. T.; Chen, Y.; Hong, Y.; Lam, J. W. Y.; Wen, Z.; Liu, W.; Zhang, W.; Zheng, L.; Tang, B. Z. Real-Time Imaging of Cell Behaviors in Living Organisms by a Mitochondria-Targeting AIE Fluorogen. *Adv. Funct. Mater.* **2016**, *26*, 7132.
(79) Ni, J.-S.; Zhang, P.; Jiang, T.; Chen, Y.; Su, H.; Wang, D.; Yu, Z.-Q.; Kwok, R. T. K.; Zhao, Z.; Lam, J. W. Y.; Tang, B. Z. Red/NIR-Emissive Benzo[D]Imidazole-Cored Aiegens: Facile Molecular Design for Wavelength Extending and in Vivo Tumor Metabolic Imaging. *Adv. Mater.* **2018**, *30*, 1805220.
(80) Zhang, R.; Duan, Y.; Liu, B. Recent Advances of AIE Dots in NIR Imaging and Phototherapy. *Nanoscale* **2019**, *11*, 19241.

(81) Zebibula, A.; Alifu, N.; Xia, L.; Sun, C.; Yu, X.; Xue, D.; Liu, L.; Li, G.; Qian, J. Ultrastable and Biocompatible NIR-Ii Quantum Dots for Functional Bioimaging. *Adv. Funct. Mater.* **2018**, *28*, 1703451.
(82) Qian, J.; Tang, B. Z. AIE Luminogens for Bioimaging and Theranostics: From Organelles to Animals. *Chem.* **2017**, *3*, 56.
(83) Reiman, E. M.; Quiroz, Y. T.; Fleisher, A. S.; Chen, K.; Velez-Pardo, C.; Jimenez-Del-Rio, M.; Fagan, A. M.; Shah, A. R.; Alvarez, S.; Arbelaez, A.; Giraldo, M.; Acosta-Baena, N.; Sperling, R. A.; Dickerson, B.; Stern, C. E.; Tirado, V.; Munoz, C.; Reiman, R. A.; Huentelman, M. J.; Alexander, G. E.; Langbaum, J. B. S.; Kosik, K. S.; Tariot, P. N.; Lopera, F. Brain Imaging and Fluid Biomarker Analysis in Young Adults at Genetic Risk for Autosomal Dominant Alzheimer's Disease in the Presenilin 1 E280a Kindred: A Case-Control Study. *Lancet Neurol.* **2012**, *11*, 1048.
(84) Horn, A.; Reich, M.; Vorwerk, J.; Li, N.; Wenzel, G.; Fang, Q.; Schmitz-Hübsch, T.; Nickl, R.; Kupsch, A.; Volkmann, J.; Kühn, A. A.; Fox, M. D. Connectivity Predicts Deep Brain Stimulation Outcome in Parkinson Disease. *Ann. Neurol.* **2017**, *82*, 67.
(85) Orrù, G.; Pettersson-Yeo, W.; Marquand, A. F.; Sartori, G.; Mechelli, A. Using Support Vector Machine to Identify Imaging Biomarkers of Neurological and Psychiatric Disease: A Critical Review. *Neurosci. Biobehav. Rev.* **2012**, *36*, 1140.
(86) He, M.; Li, D.; Zheng, Z.; Zhang, H.; Wu, T.; Geng, W.; Hu, Z.; Feng, Z.; Peng, S.; Zhu, L.; Xi, W.; Zhu, D.; Tang, B. Z.; Qian, J. Aggregation-Induced Emission Nanoprobe Assisted Ultra-Deep through-Skull Three-Photon Mouse Brain Imaging. *Nano Today* **2022**, *45*, 101536.
(87) Zhang, C.; Feng, W.; Zhao, Y.; Yu, T.; Li, P.; Xu, T.; Luo, Q.; Zhu, D. A Large, Switchable Optical Clearing Skull Window for Cerebrovascular Imaging. *Theranostics* **2018**, *8*, 2696.
(88) Goetz, K. P.; Vermeulen, D.; Payne, M. E.; Kloc, C.; McNeil, L. E.; Jurchescu, O. D. Charge-Transfer Complexes: New Perspectives on an Old Class of Compounds. *J. Mater. Chem. C* **2014**, *2*, 3065.
(89) Hong, Y.; Geng, W.; Zhang, T.; Gong, G.; Li, C.; Zheng, C.; Liu, F.; Qian, J.; Chen, M.; Tang, B. Z. Facile Access to Far-Red Fluorescent Probes with through-Space Charge-Transfer Effects for in Vivo Two-Photon Microscopy of the Mouse Cerebrovascular System. *Angew. Chem., Int. Ed.* **2022**, *61*, 202209590.
(90) Ehsani, M.; Chaichi, M. J.; Nezammeddin Hosseini, S. Comparison of Cuo Nanoparticle and Cuo/Mwcnt Nanocomposite for Amplification of Chemiluminescence Immunoassay for Detection of the Hepatitis B Surface Antigen in Biological Samples. *Sens. Actuators B Chem.* **2017**, *247*, 319.
(91) Williams, A. T. R.; Winfield, S. A.; Miller, J. N. Relative Fluorescence Quantum Yields Using a Computer-Controlled Luminescence Spectrometer. *Analyst* **1983**, *108*, 1067.
(92) Yang, Y.; Wang, S.; Lu, L.; Zhang, Q.; Yu, P.; Fan, Y.; Zhang, F. NIR-Ii Chemiluminescence Molecular Sensor for in Vivo High-Contrast Inflammation Imaging. *Angew. Chem., Int. Ed.* **2020**, *59*, 18380.
(93) Shen, H.; Sun, F.; Zhu, X.; Zhang, J.; Ou, X.; Zhang, J.; Xu, C.; Sung, H. H. Y.; Williams, I. D.; Chen, S.; Kwok, R. T. K.; Lam, J. W. Y.; Sun, J.; Zhang, F.; Tang, B. Z. Rational Design of NIR-Ii Aiegens with Ultrahigh Quantum Yields for Photo- and Chemiluminescence Imaging. *J. Am. Chem. Soc.* **2022**, *144*, 15391.
(94) Xu, R.; Zhang, P.; Shen, Q.; Zhou, Y.; Wang, Z.; Xu, Y.; Meng, L.; Dang, D.; Zhong Tang, B. AIE Nanocrystals: Emerging Nanolights with Ultra-High Brightness for Biological Application. *Coord. Chem. Rev.* **2023**, *477*, 214944.
(95) Tong, H.; Hong, Y.; Dong, Y.; Häußler, M.; Lam, J. W. Y.; Li, Z.; Guo, Z.; Guo, Z.; Tang, B. Z. Fluorescent "Light-up" Bioprobes Based on Tetraphenylethylene Derivatives with Aggregation-Induced Emission Characteristics. *Chem. Commun.* **2006**, *35*, 3705.
(96) Tong, H.; Hong, Y.; Dong, Y.; Häussler, M.; Li, Z.; Lam, J. W. Y.; Dong, Y.; Sung, H. H. Y.; Williams, I. D.; Tang, B. Z. Protein Detection and Quantitation by Tetraphenylethene-Based Fluorescent Probes with Aggregation-Induced Emission Characteristics. *J. Phys. Chem. B* **2007**, *111*, 11817.
(97) Liu, Y.; Deng, C.; Tang, L.; Qin, A.; Hu, R.; Sun, J. Z.; Tang, B. Z. Specific Detection of D-Glucose by a Tetraphenylethene-Based Fluorescent Sensor. *J. Am. Chem. Soc.* **2011**, *133*, 660.
(98) Zhao, E.; Hong, Y.; Chen, S.; Leung, C. W. T.; Chan, C. Y. K.; Kwok, R. T. K.; Lam, J. W. Y.; Tang, B. Z. Highly Fluorescent and Photostable Probe for Long-Term Bacterial Viability Assay Based on Aggregation-Induced Emission. *Adv. Healthcare Mater.* **2014**, *3*, 88.
(99) Liu, G.-J.; Zhang, Y.; Zhou, L.; Jia, L.-Y.; Jiang, G.; Xing, G.-W.; Wang, S. A Water-Soluble AIE-Active Polyvalent Glycocluster: Design, Synthesis and Studies on Carbohydrate−Lectin Interactions for Visualization of Siglec Distributions in Living Cell Membranes. *Chem. Commun.* **2019**, *55*, 9869.
(100) Cheng, Y.; Sun, C.; Ou, X.; Liu, B.; Lou, X.; Xia, F. Dual-Targeted Peptide-Conjugated Multifunctional Fluorescent Probe with Aiegen for Efficient Nucleus-Specific Imaging and Long-Term Tracing of Cancer Cells. *Chem. Sci.* **2017**, *8*, 4571.
(101) Cai, X.-M.; Lin, Y.; Li, Y.; Chen, X.; Wang, Z.; Zhao, X.; Huang, S.; Zhao, Z.; Tang, B. Z. Bioaiegens Derived from Rosin: How Does Molecular Motion Affect Their Photophysical Processes in Solid State? *Nat. Commun.* **2021**, *12*, 1773.
(102) Situ, B.; Chen, S.; Zhao, E.; Leung, C. W. T.; Chen, Y.; Hong, Y.; Lam, J. W. Y.; Wen, Z.; Liu, W.; Zhang, W.; Zheng, L.; Tang, B. Z. Real-Time Imaging of Cell Behaviors in Living Organisms by a Mitochondria-Targeting AIE Fluorogen. *Adv. Funct. Mater.* **2016**, *26*, 7132.
(103) Qin, W.; Ding, D.; Liu, J.; Yuan, W. Z.; Hu, Y.; Liu, B.; Tang, B. Z. Biocompatible Nanoparticles with Aggregation-Induced Emission Characteristics as Far-Red/near-Infrared Fluorescent Bioprobes for in Vitro and in Vivo Imaging Applications. *Adv. Funct. Mater.* **2012**, *22*, 771.
(104) Wang, Y.; Han, X.; Xi, W.; Li, J.; Roe, A. W.; Lu, P.; Qian, J. Bright AIE Nanoparticles with F127 Encapsulation for Deep-Tissue Three-Photon Intravital Brain Angiography. *Adv. Healthcare Mater.* **2017**, *6*, 1700685.
(105) Sheng, Z.; Li, Y.; Hu, D.; Min, T.; Gao, D.; Ni, J.-S.; Zhang, P.; Wang, Y.; Liu, X.; Li, K.; Zheng, H.; Tang, B. Z. Centimeter-Deep NIR-Ii Fluorescence Imaging with Nontoxic AIE Probes in Nonhuman Primates. *Research* **2020**, *2020*, 4074593.
(106) Yang, J.; Zhang, Y.; Wu, X.; Dai, W.; Chen, D.; Shi, J.; Tong, B.; Peng, Q.; Xie, H.; Cai, Z.; Dong, Y.; Zhang, X. Rational Design of Pyrrole Derivatives with Aggregation-Induced Phosphorescence Characteristics for Time-Resolved and Two-Photon Luminescence Imaging. *Nat. Commun.* **2021**, *12*, 4883.
(107) Wurthner, F. Aggregation-Induced Emission (AIE): A Historical Perspective. *Angew. Chem., Int. Ed.* **2020**, *59*, 14192.

https://doi.org/10.1021/cbmi.3c00056
Chem. Biomed. Imaging 2023, 1, 509−521